

Article

An Aptamer Biosensing Strategy for Label-Free Assay of Dual Acute Myocardial Infarction Biomarkers Built upon AuNPs/Ti₃C₂-MXenes

Xiaona Mi ^{1,2}, Huiling Li ³ and Yifeng Tu ^{2,*}¹ College of Materials Science and Engineering, Yancheng Institute of Technology, Yancheng 224051, China² College of Chemistry, Chemical Engineering and Material Science, Soochow University, Suzhou 215123, China³ The First Affiliated Hospital, Nursing College, Soochow University, Suzhou 215006, China

* Correspondence: tuyf@suda.edu.cn

Abstract: The sensitive quantification of cardiac troponin I (cTnI) and myoglobin (Myo) in blood is essential for an early emergency diagnosis of acute myocardial infarction (AMI). Attributed to AuNPs and a titanium element on the surface of the AuNPs/Ti₃C₂-MXenes hybrid, each respective aptamer strand can be immobilized on. In this work, a nanohybrid was deposited on amino-functionalized indium tin oxide (ITO) via an Au–N bond; thereafter, it could catch cTnI-specific, thiol-functionalized DNA aptamer through Au–S self-assembly or Myo-aptamer via adsorption and metal chelate interaction between phosphate groups and titanium for specific recognition. Both using [Fe(CN)₆]^{3–/4–} as a signaling probe, the differential pulse voltammetric (DPV) current of the cTnI-aptasensor decreased after binding with cTnI, while the other responded to Myo via the impedimetric measurement. These developed biosensors enable the response to the femtogram/mL level cTnI or nanogram/mL level Myo. Remarkably, the proposed aptasensors exhibit high sensitivity and specificity for targets and display great potential for applications in clinic diagnosis.

Keywords: electrochemical biosensor; aptamer; AuNPs/Ti₃C₂-MXenes; cardiac troponin I; myoglobin; acute myocardial infarction



Citation: Mi, X.; Li, H.; Tu, Y. An Aptamer Biosensing Strategy for Label-Free Assay of Dual Acute Myocardial Infarction Biomarkers Built upon AuNPs/Ti₃C₂-MXenes. *Chemosensors* **2023**, *11*, 157. <https://doi.org/10.3390/chemosensors11030157>

Academic Editor: Manel del Valle

Received: 20 January 2023

Revised: 16 February 2023

Accepted: 21 February 2023

Published: 24 February 2023



Copyright: © 2023 by the authors. Licensee MDPI, Basel, Switzerland. This article is an open access article distributed under the terms and conditions of the Creative Commons Attribution (CC BY) license (<https://creativecommons.org/licenses/by/4.0/>).

1. Introduction

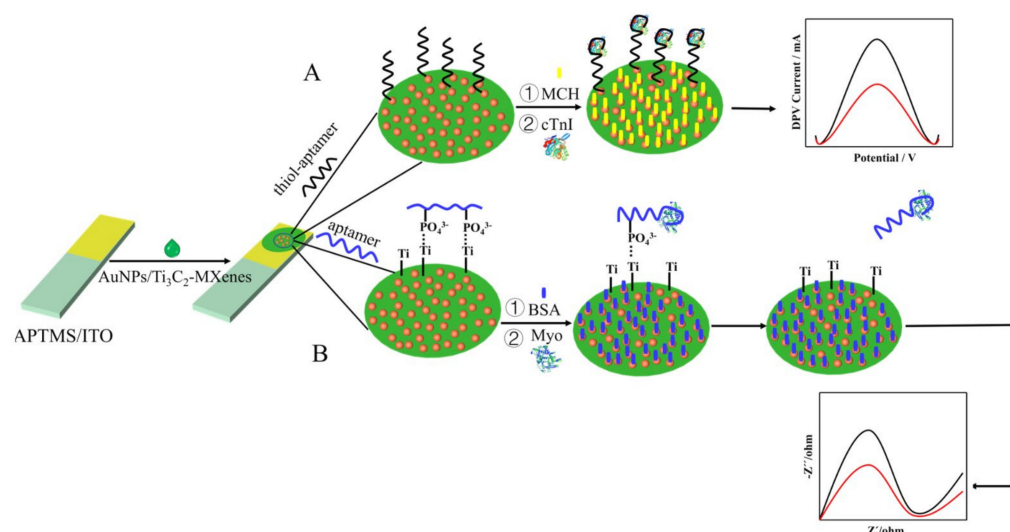
With high fatal risk, acute myocardial infarction (AMI) seriously threatens human lives as one of the most severe cardiovascular emergencies [1,2]. The early diagnosis of AMI based on the detection of cardiac biomarkers in blood is critical to guarantee the patient's survival. Clinical cardiological studies have revealed that Cardiac Troponin I (cTnI) is a gold standard biomarker due to its high cardiac specificity [3]. Compared to a normal blood level (0 to 0.01 ng/mL), it rose significantly in peripheral blood in 3–4 h after the start of an AMI attack and peaked at 12–14 h. Here, 0.01–0.04 ng/mL indicates minor myocarditis, and over 0.06 ng/mL suggests myocardial necrotic damage [4]. However, one issue is that the cTnI level is usually very low within first 2 h of the onset of symptoms and impedes the early diagnosis of AMI [5]. Recently, the multiplexed cardiac biomarker assay used in the early diagnosis of AMI has been proposed. Myoglobin (Myo) has received much attention because it is quickly released into the blood within 1 h of AMI [6]. Its concentration would drastically increase by up to 600 ng/mL within 4–5 h, while its normal range is 6–100 ng/mL [7]. Therefore, the consolidated assay of cTnI and Myo can promote responsiveness in the early diagnosis of AMI [8]. In view of the nanogram-level concentrations of cTnI and Myo in normal blood, the requirement of high sensitivity in the detection of cTnI and Myo seems to be imperative.

The typical clinical practice method for their detection in blood is usually the enzyme-linked immunosorbent assay (ELISA) [1]; however, this method is expensive, laborious, and time-consuming. More methods such as surface-enhanced Raman spectroscopy [9],

fluorescence [10], or electrochemistry [8,11] have been developed as alternatives in recent years, including various sensing methods, and electrochemical aptasensors have gained significant attention. The electrochemical techniques possess natural advantages originated from their uniqueness in principle. They generally have high sensitivity, and the response only occurs on the tiny electrode surface; therefore, only a very small sample and reagent consumption is needed, and thus the detection cost is extremely low. Moreover, electrochemical testing only takes a few seconds to some minutes, which is faster than other methods. Based on the high specificity of aptamer, the developed electrochemical sensor is basically free from the interference of coexisting substances, therefore various pretreating procedures can be ignored to directly determine the sample, which greatly simplifies the operation.

Ti₃C₂-MXene nanosheets have been employed to improve the sensitivity of electrochemical biosensors, using their assimilating metallic conductivity and excellent catalytic ability to amplify the electrical signal [12–16]. Chen et al. found that the immobilized tyrosinase on Ti₃C₂-MXene nanosheets could support a mediator-free electrochemical biosensor for an ultrasensitive and rapid detection of phenol [17]. Due to abundant transition metal (e.g., titanium) on the basal plane of Ti₃C₂-MXenes, it provides the opportunity to interact with ssDNA strands via chelation, making it a unique nano-bio-interface for biosensor construction [18]. Li et al. demonstrated that Ti₃C₂-MXene nanosheets can catch tetrahedral DNA nanostructures (TDNs) onto its surface through the coordination between titanium and phosphate groups of DNA for the highly sensitive detection of gliotoxin [19]. Recently, one report showed a more enhanced electrocatalytic activity of gold decorated Ti₃C₂-MXene nanosheets (AuNPs/Ti₃C₂-MXenes) than itself [20]. This hybrid is more likely to be a robust matrix for sensitive electrochemical detection.

The synthesized nanohybrid AuNPs/Ti₃C₂-MXenes in our previous work exhibits excellent biocompatibility and electrocatalytic activity. The AuNPs are generated in situ via the reduction of HAuCl₄ by the reducibility of activated Ti species on the surface of Ti₃C₂-MXene nanosheets [21]. The anchored AuNPs on the surface of Ti₃C₂-MXene nanosheets ensure the hybrid with improved conductivity. Moreover, the decoration of AuNPs can act as not only a spacer to prevent the pile-up of Ti₃C₂-MXene nanosheets from irreversibly restacking, but also as a connector to fix enough cTnI aptamer through the Au–S bond. Meanwhile, there is abundant titanium atoms on the basal plane of Ti₃C₂-MXene nanosheets which strongly coordinate with phosphate groups of the Myo aptamer. All these components present opportunities to construct biosensors with excellent performance. Based on this, in this work, an ultrasensitive label-free cTnI and Myo aptasensing system is developed using the leveraging of nanohybrids as the matrix for anchoring aptamer strands (Scheme 1). The nanohybrid was deposited on amino-functionalized ITO via an Au–N bond; then, the thiol-functionalized, cTnI-specific aptamer (SH-Apt_{cTnI}) was further immobilized through Au–S self-assembly, as illustrated in Scheme 1A. It is found that, after the specific binding of cTnI, the formed sensing interface showed high sensitive response toward the redox of [Fe(CN)₆]^{3−/4−} as a probe. Thus, the quantitatively decreased DPV signal is observed due to the protein layer, which inhibited the diffusion of the redox probe. Again, the adsorption of ssDNA strands on Ti₃C₂-MXene nanosheets endows its bio-affinity toward a DNA aptamer [19,22] to facilitate the development of an electrochemical aptasensor using the aptamer of Myo (Apt_{Myo}), as illustrated in Scheme 1B. The impedance of the resultant sensor diminished quickly in the presence of Myo, since the strong affinity of the specifically recognized Myo with an aptamer led to the formation of a rigid structure, resulting in its release from the sensor surface. The change in impedance bears the responsibility of the aptasensor's response to Myo. This bifunctional label-free electrochemical sensing strategy used in coupling the catalytic activity and physicochemical property of AuNPs/Ti₃C₂-MXenes with two aptamers offers a new concept for the accurate measurement of dual cardiac biomarkers in clinical diagnosis.



Scheme 1. Diagram of the preparation and operation process of aptasensor for dual cardiac biomarkers based on nano-hybrid functionalized substrate electrode. “A” represents the preparation process of the cTnI aptasensor using DPV current output upon scanning potential (V); “B” represents the preparation process of the Myo aptasensor with AC impedance (Z) as output signal.

2. Materials and Methods

2.1. Materials

Cardiac troponin I (cTnI) was purchased from Abcam Co., Ltd. (Shanghai, China). Cardiac myoglobin (Myo) was purchased from Nanjing Oukai Biotechnology Co., Ltd. (Nanjing, China). ELISA Kit for cTnI and Myo assays were purchased from Dongshang Co., Ltd. (Shanghai, China). Potassium ferricyanide ($K_3[Fe(CN)_6]$, 99.5%), potassium ferrocyanide ($K_4[Fe(CN)_6] \cdot 3H_2O$, 99.5%), and sodium chloride (NaCl) were purchased from Macklin Biochemical Co., Ltd. (Shanghai, China). BSA was obtained from Shanghai Sangon Biotech Co., Ltd. (Shanghai, China). 6-Mercapto-1-hexanol (MCH) was purchased from Sigma–Aldrich (Shanghai, China). Chloroauric acid ($HAuCl_4 \cdot 3H_2O$) was purchased from Shanghai Sinopharm Chemical Reagent Co., Ltd. (Shanghai, China). Titanium Carbide (Ti_3AlC_2 , 98%) was purchased from 11 Technology Co., Ltd. (Jilin, China). Human serum samples were collected in Second Affiliated Hospital of Soochow University (Suzhou, China) and stored under $-20^\circ C$. All other chemicals and reagents were of analytical grade. Ultrapure water (resistivity $\geq 18 M\Omega cm^{-2}$) was obtained from a Milli-Q purification system and used throughout the experiment. All oligonucleotides were synthesized by Shanghai Sangon Biotech. Co., Ltd. (Shanghai, China). The sequences of cTnI and Myo aptamers are as follows:

cTnI:

5'-SH-(CH₂)₆-CGTGCAGTACGCCAACCTTTCTCATGCGCTGCCCTCTTA-3' [23].

Myo:

5'-CCCTCCTTTCCTTCGACGTAGATCTGCTGCGTTGTTCCGA-3' [22].

0.1 M PBS solution (pH 7.0) was prepared by the mix of stock solutions of 0.1 M Na_2HPO_4 and 0.1 M NaH_2PO_4 in a specific proportion. The stock aptamer solution of cTnI or Myo was prepared using the aqua solution containing 10 mM Tris-HCl and 50 mM $MgCl_2$ (pH = 7.4). The immobilization of the aptamer was manipulated afterwards to dilute the stock solution with 0.1 M phosphate-buffered saline (PBS) (pH 7.0).

2.2. Apparatus

All electrochemical experiments were carried out using a conventional three-electrode system with an ITO-based working electrode or sensor, a Pt wire counter electrode, and a saturated calomel electrode (SCE) as a reference electrode. Electrochemical impedance spectroscopy (EIS), cyclic voltammetry (CV), and differential pulse voltammetry (DPV)

were enforced on an RST-5200 Electrochemical Workstation (Risetest Instruments of Suzhou, Suzhou, China). All the electrochemical tests were carried out in 0.1 M PBS (pH 7.0) containing 5 mM $[\text{Fe}(\text{CN})_6]^{3-/4-}$ and 0.1 M NaCl. The CV measurements were implemented in a potential range from -0.2 to 0.6 V with a scanning rate of 50 mV/s. The DPV measurements were performed in a potential range from -0.3 to 0.7 V under the following conditions: a pulse amplitude of 100 mV, a pulse width of 20 ms, and a sampling width of 10 ms. EIS measurements were performed in the frequency range of 0.1 – 10^5 Hz. The atomic force microscopy (AFM) characterization was fulfilled using Dimension Icon Atomic Force Microscopy (Bruker, Germany). Those images were taken in tapping mode using an RTP cantilever (7 nm of tip radius, 2 N/m of elastic coefficient).

2.3. Fabrication of Aptamer/AuNPs/Ti₃C₂-MXenes Aptasensors

The synthesis of the AuNPs/Ti₃C₂-MXene hybrid, pretreatment of ITO glass, and the preparation of amino-functionalized ITO (APTMS/ITO) all can refer to our previous paper [20]. For the fabrication of the aptamer/AuNPs/Ti₃C₂-MXene biosensors, 50 μL of as-prepared AuNPs/Ti₃C₂-MXene hybrid suspension was dropped onto the surface of the APTMS/ITO electrode and left for 30 min at room temperature, which, when followed by washing with ultrapure water and dried under N₂ gas flow, gained a AuNPs/Ti₃C₂-MXenes/APTMS/ITO electrode. Subsequently, 10 μL of aptamer solution was cast onto it before waiting for 12 h at 4 °C to fix the aptamer (Apt/AuNPs/Ti₃C₂-MXenes/APTMS/ITO). Thereafter, for the cTnI aptasensor, 10 μL of 10 mM MCH (in 0.1 M PBS, pH 7.0) solution was necessary to treat the sensor for 30 min to block the unoccupied sites and prevent the entanglement of ssDNA aptamers; moreover, for the Myo aptasensor, 10 μL of 3% BSA (in 0.1 M PBS, pH 7.0) solution was placed on the resulting electrode for 30 min to block the unoccupied sites. Lastly, the obtained aptasensors were stored at 4 °C for further use.

2.4. cTnI and Myo Detection

A total of 10 μL of the sample solution was placed onto the aptasensor and incubated at 25 °C for 60 min before being washed with 0.1 M PBS (pH 7.4). Then, the sensor was imbedded into the electrochemical cell for DPV or EIS measurement.

3. Results and Discussion

3.1. Monitoring the Preparation of Aptasensors

The preparation and characterization of the AuNPs/Ti₃C₂-MXene hybrid, as well as its use to prepare the basal electrode of the aptasensors, have been presented in our previous paper [20]. Here, the interfacial character of the aptasensor in different preparing steps was explored using AFM (Figure 1A). The AFM image of a bare ITO electrode shows a grainy topology (Figure 1Aa) with an average surface roughness (R) of 5.74 nm. Thereafter, it (Figure 1Ab) revealed a smoother surface with a decreased R value of 4.66 nm when the ITO was covered using APTMS. After the AuNPs/Ti₃C₂-MXene hybrid was deposited on, the surface became much rougher (Figure 1Ac), as indicated by a significantly increased R value of 10.30 nm. The anchoring of the aptamer (as thiol–Apt_{cTnI}) induced a larger R value (Figure 1Ad, 15.10 nm), proving that lots of aptamer strands were attached onto the surfaces of the AuNPs/Ti₃C₂-MXenes through the Au–S bond [24]. As illustrated in Figure 1Ae, after treatment with MCH, the R value increased by up to 23.10 nm, indicating a much rougher morphology, which can be attributed to the fact that MCH would regulate the orientation of the ssDNA aptamer, which tended to arrange them vertically [25]. After this, to incubate the cTnI (Figure 1Af) on a sensor, a smoother morphology than the one displayed in Figure 1Ae, with a decreased R value of 18.70 nm, was observed as a result of the connection of globular and high molecular weight proteins [26]. The alteration of the surface roughness of the electrode during the preparation process indicated the successful construction of the aptasensor.

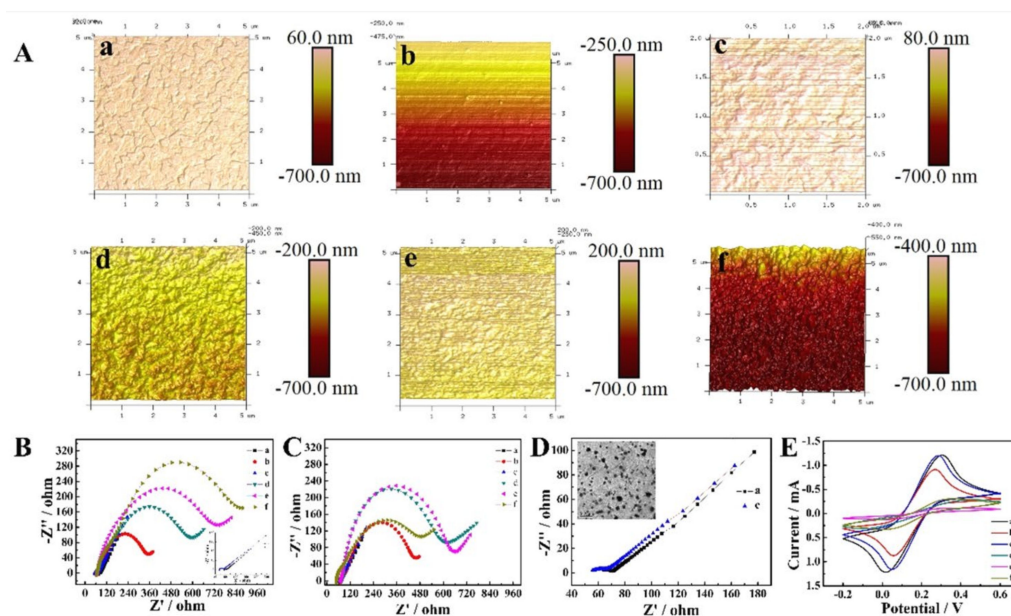


Figure 1. (A) Three-dimensional AFM images and (B) EIS curves of (a) bare ITO, (b) APTMS/ITO, (c) AuNPs/Ti₃C₂-MXenes/APTMS/ITO, (d) after to catch cTnI aptamer, (e) final cTnI sensor, and (f) responded to cTnI, the inset in (B) shows the enlarged EIS curves (a) and (c); (C,D) EIS curves and (E) CV curves of [Fe(CN)₆]^{3−/4−} on (a) bare ITO, (b) APTMS/ITO, (c) AuNPs/Ti₃C₂-MXenes/APTMS/ITO, (d) after to catch Myo aptamer, (e) final Myo sensor, and (f) responded to Myo, the inset in (D) is the TEM image of AuNPs/Ti₃C₂-MXenes.

Moreover, the EIS and CV can reflect the process of sensor preparation. As shown in Figure 1B–E, the electron transfer resistance (R_{et} , it can be obtained from the equivalent circuit of the semi-circular part of EIS, which represents the impedance of the electrode surface for electron transfer) significantly increased, and the CV current obviously decreased after covering the bare ITO with hydrolyzed APTMS due to its electro-inactive feature [27] (both curves a and b). In contrast, obviously decreased R_{et} and increased CV currents (both curve c) were witnessed after the decoration of the AuNPs/Ti₃C₂-MXenes (the microscopic image of TEM is presented in Figure 1D), suggesting better conductivity and a larger specific surface area. Afterwards, the R_{et} values increased once more when the aptamer (thiol-Apt_{cTnI} or Apt_{Myo}) was fixed (curve d), or when the CV currents decreased in reverse after the successive linkage of the aptamer (as Apt_{Myo}) (curve d). When treating the cTnI sensor with MCH or the Myo sensor with BSA (both curve e), the EIS of the former increased due to the molecular orientation [25], and the latter experienced minor changes; moreover, the CV current of the latter slightly decreased due to the hampered electron transfer [28]. Finally, if the cTnI sensor had been used to detect the target, the readout signal (EIS) would further increase according to the concentration (curve f in Figure 1B); whereas, for the Myo sensor, the EIS decreased (curve f in Figure 1C), and the CV current recovered in degree (curve f in Figure 1E). These results suggest that all components of the aptasensor were successfully integrated and endowed with the desired sensing ability as expected.

3.2. Optimization of the Conditions for Sensor Preparation and Operation

The dosage of the AuNPs/Ti₃C₂-MXene hybrid significantly influences the performance of the aptasensor [7]. As shown in Figure 2A (black curve), the DPV signal is elevated along with the increasing dosage of the AuNPs/Ti₃C₂-MXene hybrid, reaching a maximum of 0.25 mg/mL, when then declined if further enlarged. This implies that overdosing the hybrid on the electrode surface would inversely impede the electron transfer, owing to more serious interface resistance [29]. Using EIS, the dosage of the AuNPs/Ti₃C₂-MXene hybrid can be optimized too, acquired a result of 0.25 mg/mL, which led to a smallest R_{et} (Figure 2A, blue curve) that was totally identical to the results obtained using DPV.

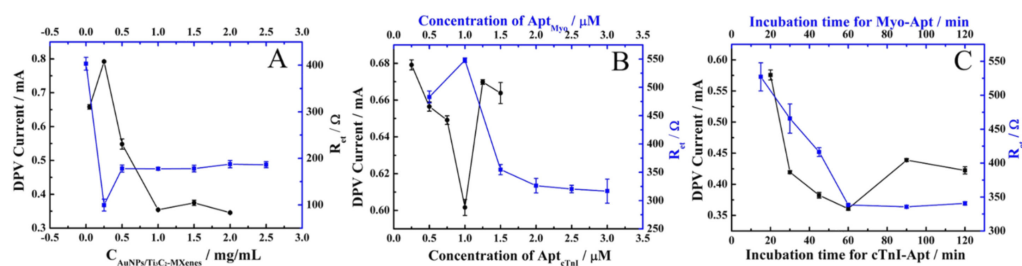


Figure 2. The optimization (A) and the content of AuNPs/Ti₃C₂-MXenes; (B) the concentration of Apt_{cTnI} or Apt_{Myo}; (C) the time for cTnI or Myo incubation.

SH-Apt_{cTnI} is used as a recognitive host for cTnI, and its quantitative use also must be optimized to achieve a maximal sensing outcome. As depicted in Figure 2B (black curve), with the same used volume, the minimal DPV peak current of [Fe(CN)₆]^{3−/4−} was observed when the concentration of SH-Apt_{cTnI} for enabling the sensor was 1.0 μM . This means that this usage quantity is likely to ensure a binding saturation, and we speculate that an excess of SH-Apt_{cTnI} is prone to lead to its detachment, eventually being detrimental to the analytical performance of the resulting sensor [30]. Similarly, the most suitable concentration of the Apt_{Myo} solution for Myo aptasensor construction was also 1.0 μM (Figure 2B blue curve).

Meanwhile, the incubation time of the target of the corresponding aptasensor is also an important factor when aiming to achieve the best sensing performance. As shown in Figure 2C (black curve), a very significant decrease in DPV value occurs after the loading of the cTnI sample solution within an incubation time of 60 min, suggesting that the binding of cTnI on its aptamer reached a full equilibrium during this period [31]. The results indicate that the longer time negatively affected the performance of the aptasensor. Consistently, the optimal incubation time for the Myo aptasensor is also 60 min (Figure 2C blue curve).

3.3. The Analytical Performance of Prepared Aptasensors

Under the optimal conditions, the analytical performance of the proposed aptasensing strategy was validated by detecting cTnI or Myo.

Figure 3A shows that the DPV current on the prepared Apt_{cTnI} sensor gradually decreased along with elevating the cTnI concentration. This is attributed to the insulativity of the formed aptamer–cTnI complex, which obstructed the electron transfer between the electrochemical probe and the AuNPs/Ti₃C₂-MXene substrate electrode [8]. There was a good linear regression of the DPV peak current upon the logarithm of the cTnI concentration from 0.24 fg/mL to 24 ng/mL, as illustrated in Figure 3B, which perfectly covers the clinically relevant range. The linear regression equation is $I = 0.456 - 0.0177 \log C$ (fg/mL) ($R^2 = 0.999$), with a limit of detection (LOD) of 0.14 fg/mL ($S/N = 3$). Visibly, the LOD of the prepared Apt_{cTnI} sensor lays well below the normal level of cTnI and can easily identify the myocardial necrotic damage.

Table 1 lists the performance of the proposed aptasensor and offers a comparison between it and other currently available cTnI sensors. The results reveal that the developed aptasensor possesses a higher sensitivity than all other reported ones. This is mainly ascribed to the following aspects: (i) the superior electrochemical activity of the AuNPs/Ti₃C₂-MXenes greatly promotes the electron transfer and amplifies the response; (ii) the prepared AuNPs/Ti₃C₂-MXene hybrid has excellent biocompatibility, which can strengthen aptamer anchoring using the Au–S bond; (iii) SH-Apt_{cTnI} possesses a highly specific and sensitive recognition toward cTnI.

Surprisingly, after the Myo is specifically recognized by the aptasensor, the R_{et} value decreased, whereas the CV current increased, respectively (curve f in Figure 1C,E). This suggests that the electron transfer on the sensing interface was recovered. This can only be because the peeled off of Apt_{Myo} from sensor surface due to the formation of the aptamer–Myo complex. As the result, the sensor can feasibly facilitate the highly sensitive detection

capability of Myo because the degree of its output recovery strongly depends on the concentration of the target.

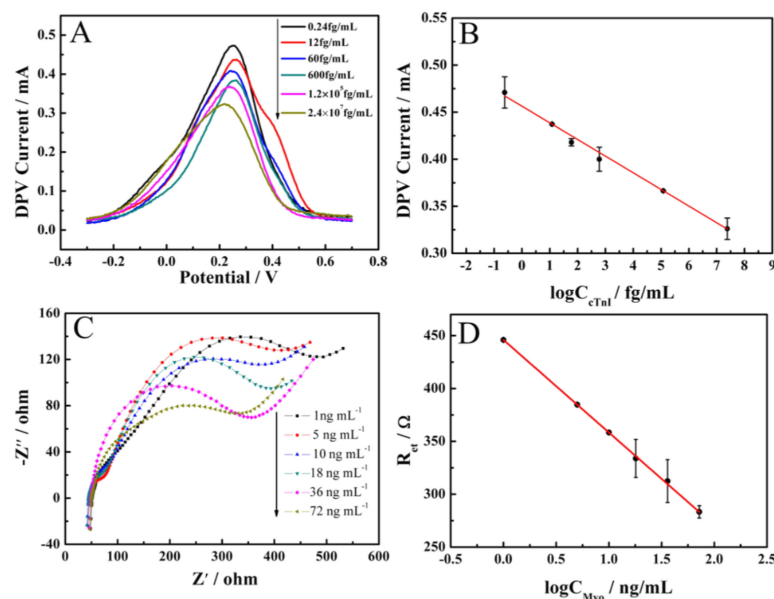


Figure 3. (A) The DPV responses of Apt_{cTnI} sensor for detecting cTnI. (B) The linear relationship between DPV current and the logarithm of cTnI concentration. (C) The EIS responses of Apt_{Myo} sensor for detecting Myo. (D) The linear relationship between Ret and the logarithm of Myo concentration.

Table 1. Performance comparison of the developed sensor with those in the literature for cTnI and Myo detection.

Electrode Materials	Target	Method	Detection Range	LOD	Refs.
HsGDY@NDs	cTnI	EIS	0.01 pg/mL–100 ng/mL	6.29 fg/mL	[8]
Fc-SiNP		SWV	0.024 ng/mL–240 ng/mL	24 pg/mL	[23]
Ti/AuNPs		DPV	0.024 ng/mL–26.4 ng/mL	4.32 pg/mL	[32]
Fc-COFNs		DPV	10 fg/mL–10 ng/mL	2.6 fg/mL	[33]
PCN-AuNPs		SWV	0.1 pg/mL–103 ng/mL	0.01 pg/mL	[2]
Au/Zr-C		i-t	0.01 pg/mL–100 ng/mL	1.24 fg/mL	[34]
Pt@Pd DNs/NH ₂ -HMCS		i-t	100 fg/mL–100 ng/mL	15.4 fg/mL	[35]
AuNPs/Ti ₃ C ₂ -MXenes		DPV	0.24 fg/mL–24 ng/mL	0.14 fg/mL	This work
AuNPs/BNNSs		DPV	0.1 μg/mL–100 μg/mL	34.6 ng/mL	[36]
DApt-CS conjugate		DPV	1.67 ng/mL–666.67 ng/mL	0.45 ng/mL	[37]
Poly-o-phenylenediamine	Myo	DPV	10 ng/mL–1780 ng/ml	10 ng/mL	[38]
AuNP-PEI		SWV	9.96 ng/mL–72.8 ng/mL	6.29 ng/mL	[39]
magnetic beads		GMI	1 ng/mL–10 ng/mL	0.5 ng/mL	[40]
AuNPs@rGO		DPV	1 ng/mL–1400 ng/mL	0.67 ng/mL	[41]
AuNPs/Ti ₃ C ₂ -MXenes		EIS	1 ng/mL–70 ng/mL	0.2 ng/mL	This work

The analysis of Myo was carried out under optimal conditions using the EIS test. Figure 3C shows the EIS responses of aptasensor after being incubated with differently concentrated Myo. It can be observed that the R_{et} value of the aptasensor is regressively decreased upon increasing Myo concentration. In Figure 3D, a good linear relationship (R² = 0.999) was obtained between the R_{et} and the logarithm of the Myo concentration (log C_{Myo}) in a range of 1–72 ng/mL. The linear regression equation is R_{et} = 446 – 87.6 log C (ng/mL) with an LOD of 0.2 ng/mL (S/N = 3), which also lays well below the normal value of Myo in blood. This Apt_{Myo}/AuNPs/Ti₃C₂-MXene-hosted sensor exhibits superior analytical performance compared with other bioassays for Myo, as listed in Table 1. Remarkably, the low LOD of the designed aptasensor highlights the potential role of AuNPs/Ti₃C₂-MXenes in biosensing territory.

3.4. Specificity, Stability and Reproducibility of the Proposed Aptasensors

A diagnostic biosensor must possess high specificity for a target molecule against other interfering materials. Therefore, the specificity of the AuNPs/Ti₃C₂-MXene-based aptasensors for detecting their respective target were evaluated in the presence of 100-fold high concentrated inspected materials, including C-reactive protein (CRP), Albumin (Alb) and N-terminal pro-brain nitric peptide (NT-pro-BNP), as well as Myo or cTnI, and their mixture with cTnI or Myo was also examined. Except the corresponding target, the response of the coexistent biomolecules was almost zero, as illustrated in Figure 4A,D. These results indicate the high specificity of both two electrochemical aptasensors, which is apparently from the proper specific aptamer on the modified electrode.

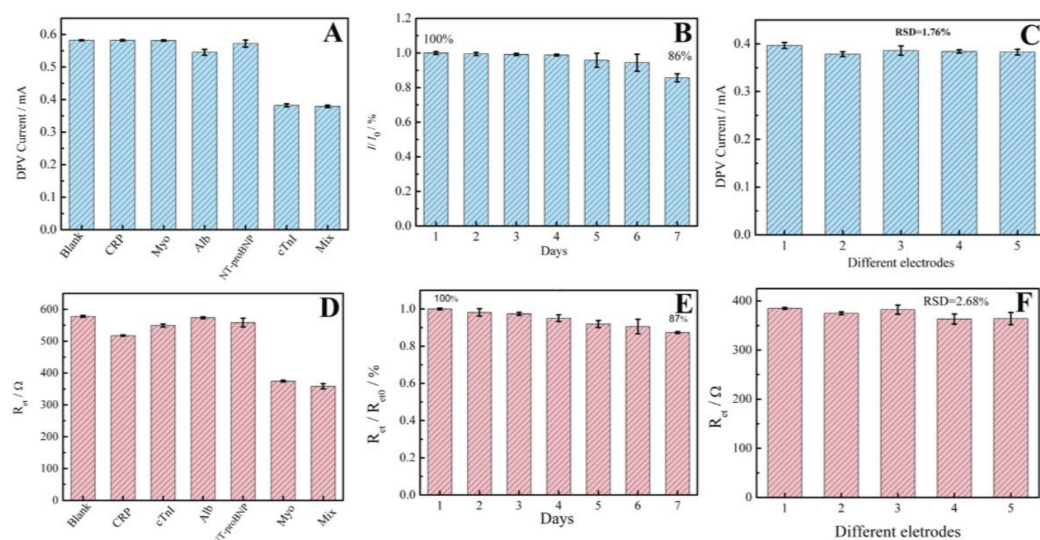


Figure 4. The (A) selectivity (in the presence of 60 pg /mL CRP, Myo, Alb and NT-proBNP), (B) stability and (C) reproducibility of the cTnI aptasensor for cTnI (600 fg/mL) detection, all detected values are presented as blue bars. The (D) selectivity (in the presence of 50 ng/mL CRP, cTnI, Alb and NT-proBNP), (E) stability and (F) reproducibility of the Myo aptasensor for Myo (5 ng/mL) detection, all detected values are presented as red bars.

The storage stability of the developed aptasensors was examined by monitoring their response toward cTnI or Myo once per day. The results show that they retained up to 86% to 87% of their initial responses after seven days of use, respectively (Figure 4B,E). The aptasensors showed good reproducibility for 1.76% or 2.68% of RSD for five parallel prepared sensors, respectively, as illustrated in Figure 4C,F. The appreciable stability and reproducibility stem from the effective immobilization efficiency of aptamers on AuNPs/Ti₃C₂-MXene-modified electrodes through interactions such as the covalent linkage of Au-S and perhaps existing chelation between the Ti of AuNPs/Ti₃C₂-MXenes and PO₄³⁻ of the DNA aptamer.

3.5. Detection of cTnI or Myo in Human Serum Sample

To explore the practicability of developed aptasensors, they were used to detect cTnI or Myo in real human serum samples, with the recovery test using a standard addition method (Table 2). Plainly, the recovery of the cTnI aptasensor is in the range of 99.0–106% (RSD in the range of 0.60–1.98%). The recovery for Myo ranges from 92.0% to 108% (RSD in the range of 1.40–5.50%). The results demonstrate that the sensors were feasibly able to determine cTnI or Myo in human serum. The accuracy of the designed aptasensors was also verified by comparing the results with enzyme-linked immunosorbent assay (ELISA). As listed in Table 2, the contents of cTnI and Myo in four human serum samples detected using the proposed sensors were in good agreement with that of the ELISA.

Table 2. Quantitative results of cTnI and Myo in human serum samples.

Sample	Found cTnI (ng/mL)	Added cTnI (ng/mL)	Total Detected cTnI (ng/mL)	Recovery (%)	ELISA (ng/mL)	RSD (%)
1	0.0667 ± 0.0028	0.01	0.0773 ± 0.0015	106	0.07	1.98
2	0.110 ± 0.007	0.01	0.120 ± 0.001	100	0.09	0.61
3	0.0121 ± 0.0010	0.01	0.0220 ± 0.0020	99.0	<0.029	0.91
4	0.0243 ± 0.0021	0.01	0.0344 ± 0.0020	101	<0.029	0.60
Sample	Found Myo (ng/mL)	Added Myo (ng/mL)	Total Detected Myo (ng/mL)	Recovery (%)	ELISA (ng/mL)	RSD (%)
1	15.5 ± 0.39	5.0	20.7 ± 1.13	104	15.7	5.50
2	24.9 ± 0.63	5.0	29.5 ± 0.75	92.0	25.0	2.54
3	69.6 ± 0.60	0.5	70.1 ± 0.98	100	70.1	1.40
4	14.1 ± 0.10	5.0	19.5 ± 1.06	108	14.1	5.43

4. Conclusions

The bifunctional and label-free electrochemical aptasensing strategy with AuNPs/Ti₃C₂-MXenes as substrate has been investigated for the sensitive quantification of the dual biomarkers of AMI disease, cTnI and Myo. The AuNPs/Ti₃C₂-MXene hybrid not only serves as a matrix to anchor the aptamer, but also provides excellent electroactivity to accelerate the electron transfer to promote the sensing ability of the aptasensors. Both using [Fe(CN)₆]^{4−/3−} as redox probe, the cTnI aptasensor shows a high DPV response with a low LOD of 0.14 fg/mL and a wide linear range; meanwhile, the Myo assay is successful from the recovered EIS due to the detachment of the Myo aptamer, which acquired a low LOD of 0.2 ng/mL. Of course, the specificity of the two sensors is also excellent because of the high recognition of the target by the aptamer. Besides the high sensitivity and specificity, what is more meaningful is that the designed aptasensors are label-free ones; thus, they are simpler and quicker in response than that of the ELISA method, which was based on the labeling technique. However, so far, we can only operate on two sensors separately, due to the limitation of the function of the equipment. What we are reporting here is only a phased work, and its purpose is to verify the feasibility of these dual biomarkers' synchronous detection. As for its application in the real world, it still depends on further development and research. This will not hinder the application of this technology, as long as the equipment is upgraded. According to our study, an array composed of two sensors can feasibly solve the problem of the synchronous detection of two biomarkers in a single operation. Only needs an implemented macro instruction on the instrument to start each sensor in a time-sharing with a jumper circuit which is used to realize the gating of the sensors. Alternatively, the two sensors can be submerged totally with each other, because they adopt a different driving principle and do not interfere with each other. This research suggests that the proposed aptasensing strategy might be a promising platform for the early and accurate screening and diagnosis of AMI in clinical applications.

Author Contributions: Experiment, Data analysis, writing—original draft, X.M.; investigation, conceptualization, Writing—review and editing, H.L.; project instruction, design and methodology, experimental verification, writing—review and editing, funding acquisition, Y.T. All authors have read and agreed to the published version of the manuscript.

Funding: This work is financially supported by the National Natural Science Foundation of China (21675115, 21375091).

Institutional Review Board Statement: Not applicable.

Informed Consent Statement: Not applicable.

Data Availability Statement: Not applicable.

Conflicts of Interest: The authors declare no conflict of interest.

References

1. Ji, J.; Lu, W.; Zhu, Y.; Jin, H.; Yao, Y.; Zhang, H.; Zhao, Y. Porous Hydrogel-Encapsulated Photonic Barcodes for Multiplex Detection of Cardiovascular Biomarkers. *ACS Sens.* **2019**, *4*, 1384–1390. [[CrossRef](#)] [[PubMed](#)]
2. Khushaim, W.; Peramaiah, K.; Beduk, T.; Vijjapu, M.T.; Filho, J.I.D.O.; Huang, K.-W.; Mani, V.; Salama, K.N. Porous graphitic carbon nitrides integrated biosensor for sensitive detection of cardiac troponin I. *Biosens. Bioelectron. X* **2022**, *12*, 100234. [[CrossRef](#)]
3. Mi, X.; Li, H.; Tan, R.; Tu, Y. Dual-Modular Aptasensor for Detection of Cardiac Troponin I Based on Mesoporous Silica Films by Electrochemiluminescence/Electrochemical Impedance Spectroscopy. *Anal. Chem.* **2020**, *92*, 14640–14647. [[CrossRef](#)] [[PubMed](#)]
4. Yuan, Z.; Wang, L.; Chen, J.; Su, W.; Li, A.; Su, G.; Liu, P.; Zhou, X. Electrochemical strategies for the detection of cTnI. *Anal.* **2021**, *146*, 5474–5495. [[CrossRef](#)]
5. Maisel, A.; Mueller, C.; Neath, S.-X.; Christenson, R.H.; Morgenthaler, N.G.; McCord, J.; Nowak, R.M.; Vilke, G.; Daniels, L.B.; Hollander, J.E.; et al. Copeptin Helps in the Early Detection of Patients with Acute Myocardial Infarction. *J. Am. Coll. Cardiol.* **2013**, *62*, 150–160. [[CrossRef](#)]
6. Yoo, S.S.; Kim, S.Y.; Kim, K.S.; Hong, S.; Oh, M.J.; Nam, M.G.; Kim, W.-J.; Park, J.; Chung, C.-H.; Choe, W.-S.; et al. Controlling inter-sheet-distance in reduced graphene oxide electrodes for highly sensitive electrochemical impedimetric sensing of myoglobin. *Sens. Actuators B Chem.* **2020**, *305*, 127477. [[CrossRef](#)]
7. Zhang, J.X.; Tang, C.; Chen, D.N.; Jiang, L.Y.; Wang, A.J.; Feng, J.J. Ultrasensitive Label-Free Sandwich Immunoassay of Cardiac Biomarker Myoglobin Using Meso-SiO₂@Ploydapamine@PtPd Nanocrystals and PtNi Nanodendrites for Effective Signal Amplification. *Appl. Surf. Sci.* **2023**, *608*, 155216. [[CrossRef](#)]
8. Wang, C.; Li, J.; Kang, M.; Huang, X.; Liu, Y.; Zhou, N.; Zhang, Z. Nanodiamonds and hydrogen-substituted graphdiyne heteronanostructure for the sensitive impedimetric aptasensing of myocardial infarction and cardiac troponin I. *Anal. Chim. Acta* **2021**, *1141*, 110–119. [[CrossRef](#)]
9. Zhang, D.; Huang, L.; Liu, B.; Su, E.B.; Chen, H.Y.; Gu, Z.Z.; Zhao, X.W. Quantitative Detection of Multiplex Cardiac Bi-omarkers with Encoded SERS Nanotags on a Single T Line in Lateral Flow Assay. *Sens. Actuators B* **2018**, *277*, 502–509. [[CrossRef](#)]
10. Guo, X.; Zong, L.; Jiao, Y.; Han, Y.; Zhang, X.; Xu, J.; Li, L.; Zhang, C.-W.; Liu, Z.; Ju, Q.; et al. Signal-Enhanced Detection of Multiplexed Cardiac Biomarkers by a Paper-Based Fluorogenic Immunodevice Integrated with Zinc Oxide Nanowires. *Anal. Chem.* **2019**, *91*, 9300–9307. [[CrossRef](#)]
11. Wang, B.; Shi, S.W.; Yang, X.L.; Wang, Y.; Qi, H.L.; Gao, Q.; Zhang, C.X. Separation-Free Electrogenerated Chemiluminescence Immunoassay Incorporating Target Assistant Proximity Hybridization and Dynamically Competitive Hybridization of a DNA Signal Probe. *Anal. Chem.* **2020**, *92*, 884–891. [[CrossRef](#)]
12. Alwarappan, S.; Nesakumar, N.; Sun, D.; Hu, T.Y.; Li, C.-Z. 2D metal carbides and nitrides (MXenes) for sensors and biosensors. *Biosens. Bioelectron.* **2022**, *205*, 113943. [[CrossRef](#)] [[PubMed](#)]
13. Lorencova, L.; Gajdosova, V.; Hroncekova, S.; Bertok, T.; Blahutova, J.; Vikartovska, A.; Parrakova, L.; Gemeiner, P.; Kasak, P.; Tkac, J. 2D MXenes as Perspective Immobilization Platforms for Design of Electrochemical Nanobiosensors. *Electroanalysis* **2019**, *31*, 1833–1844. [[CrossRef](#)]
14. Aguedo, J.; Lorencova, L.; Barath, M.; Farkas, P.; Tkac, J. Electrochemical Impedance Spectroscopy on 2D Nanomaterial MXene Modified Interfaces: Application as a Characterization and Transducing Tool. *Chemosensors* **2020**, *8*, 127–148. [[CrossRef](#)]
15. Zhang, H.X.; Zhuang, T.T.; Wang, L.; Du, L.; Xia, J.F.; Wang, Z.H. Efficient Au Nanocluster@Ti₃C₂ Heterostructure Lumino-phore Combined with Cas12a for Electrochemiluminescence Detection of miRNA. *Sens. Actuators B* **2022**, *370*, 132428. [[CrossRef](#)]
16. Wei, Z.H.; Zhang, H.X.; Wang, Z.H. High-Intensity Focused Ultrasound Combined with Ti₃C₂-TiO₂ to Enhance Electrochemiluminescence of Luminol for the Sensitive Detection of Polynucleotide Kinase. *ACS Appl. Mater. Interfaces* **2023**, *15*, 3804–3811. [[CrossRef](#)]
17. Wu, L.; Lu, X.; Dhanjai; Wu, Z.-S.; Dong, Y.; Wang, X.; Zheng, S.; Chen, J. 2D transition metal carbide MXene as a robust biosensing platform for enzyme immobilization and ultrasensitive detection of phenol. *Biosens. Bioelectron.* **2018**, *107*, 69–75. [[CrossRef](#)]
18. Zhang, Q.; Wang, F.; Zhang, H.; Zhang, Y.; Liu, M.; Liu, Y. Universal Ti₃C₂ MXenes Based Self-Standard Ratiometric Fluorescence Resonance Energy Transfer Platform for Highly Sensitive Detection of Exosomes. *Anal. Chem.* **2018**, *90*, 12737–12744. [[CrossRef](#)]
19. Wang, H.; Li, H.; Huang, Y.; Xiong, M.H.; Wang, F.; Li, C. A Label-Free Electrochemical Biosensor for Highly Sensitive De-tection of Gliotoxin based on DNA Nanostructure/MXene Nanocomplexes. *Biosens. Bioelectron.* **2019**, *142*, 111531. [[CrossRef](#)]
20. Mi, X.N.; Li, H.; Tan, R.; Feng, B.N.; Tu, Y.F. The TDs/Aptamer cTnI Biosensors based on HCR and Au/Ti₃C₂-MXene Amplification for Screening Serious Patient in COVID-19 Pandemic. *Biosens. Bioelectron.* **2021**, *192*, 113482. [[CrossRef](#)]
21. Wang, L.; Zhang, H.; Zhuang, T.; Liu, J.; Sojic, N.; Wang, Z. Sensitive electrochemiluminescence biosensing of polynucleotide kinase using the versatility of two-dimensional Ti₃C₂TX MXene nanomaterials. *Anal. Chim. Acta* **2022**, *1191*, 339346. [[CrossRef](#)] [[PubMed](#)]
22. Wang, Q.; Liu, W.; Xing, Y.; Yang, X.; Wang, K.; Jiang, R.; Wang, P.; Zhao, Q. Screening of DNA Aptamers against Myoglobin Using a Positive and Negative Selection Units Integrated Microfluidic Chip and Its Biosensing Application. *Anal. Chem.* **2014**, *86*, 6572–6579. [[CrossRef](#)] [[PubMed](#)]
23. Jo, H.; Gu, H.; Jeon, W.; Youn, H.; Her, J.; Kim, S.-K.; Lee, J.; Shin, J.H.; Ban, C. Electrochemical Aptasensor of Cardiac Troponin I for the Early Diagnosis of Acute Myocardial Infarction. *Anal. Chem.* **2015**, *87*, 9869–9875. [[CrossRef](#)] [[PubMed](#)]

24. Lu, H.-J.; Pan, J.-B.; Wang, Y.-Z.; Ji, S.-Y.; Zhao, W.; Luo, X.-L.; Xu, J.-J.; Chen, H.-Y. Electrochemiluminescence Energy Resonance Transfer System between RuSi Nanoparticles and Hollow Au Nanocages for Nucleic Acid Detection. *Anal. Chem.* **2018**, *90*, 10434–10441. [[CrossRef](#)] [[PubMed](#)]
25. Zhao, F.; Xie, Q.; Xu, M.; Wang, S.; Zhou, J.; Liu, F. RNA aptamer based electrochemical biosensor for sensitive and selective detection of cAMP. *Biosens. Bioelectron.* **2015**, *66*, 238–243. [[CrossRef](#)]
26. Mishra, S.K.; Kumar, D.; Biradar, A.M.; Rajesh. Electrochemical Impedance Spectroscopy Characterization of Mercapto-propionic Acid Capped ZnS Nanocrystal Based Bioelectrode for the Detection of the Cardiac Biomarker—Myoglobin. *Bioelectrochemistry* **2012**, *88*, 118–126. [[CrossRef](#)]
27. Li, D.; Tan, R.; Mi, X.; Fang, C.; Tu, Y. An electrochemiluminescent biosensor for noninvasive glucose detection based on cluster-like AuAg hollowed-nanoparticles. *Microchem. J.* **2021**, *167*, 106271. [[CrossRef](#)]
28. Ge, X.-Y.; Zhang, J.-X.; Feng, Y.-G.; Wang, A.-J.; Mei, L.-P.; Feng, J.-J. Label-free electrochemical biosensor for determination of procalcitonin based on graphene-wrapped Co nanoparticles encapsulated in carbon nanobrushes coupled with AuPtCu nanodendrites. *Microchim. Acta* **2022**, *189*, 110. [[CrossRef](#)]
29. Lv, H.; Li, Y.; Zhang, X.; Li, X.; Xu, Z.; Chen, L.; Li, D.; Dong, Y. Thionin functionalized signal amplification label derived dual-mode electrochemical immunoassay for sensitive detection of cardiac troponin I. *Biosens. Bioelectron.* **2019**, *133*, 72–78. [[CrossRef](#)]
30. Rauf, S.; Mani, V.; Lahcen, A.A.; Yuvaraja, S.; Beduk, T.; Salama, K.N. Binary transition metal oxide modified laser-scribed graphene electrochemical aptasensor for the accurate and sensitive screening of acute myocardial infarction. *Electrochim. Acta* **2021**, *386*, 138489. [[CrossRef](#)]
31. Dong, L.; Yin, L.; Tian, G.; Wang, Y.; Pei, H.; Wu, Q.; Cheng, W.; Ding, S.; Xia, Q. An enzyme-free ultrasensitive electrochemical immunosensor for calprotectin detection based on PtNi nanoparticles functionalized 2D Cu-metal organic framework nanosheets. *Sens. Actuators B* **2020**, *308*, 127687. [[CrossRef](#)]
32. Lopa, N.S.; Rahman, M.; Ahmed, F.; Ryu, T.; Sutradhar, S.C.; Lei, J.; Kim, J.; Kim, D.H.; Lee, Y.H.; Kim, W. Simple, low-cost, sensitive and label-free aptasensor for the detection of cardiac troponin I based on a gold nanoparticles modified titanium foil. *Biosens. Bioelectron.* **2019**, *126*, 381–388. [[CrossRef](#)]
33. Song, Z.; Song, J.; Gao, F.; Chen, X.; Wang, Q.; Zhao, Y.; Huang, X.; Yang, C.; Wang, Q. Novel electroactive ferrocene-based covalent organic frameworks towards electrochemical label-free aptasensors for the detection of Cardiac Troponin I. *Sens. Actuators B* **2022**, *368*, 132205. [[CrossRef](#)]
34. Chen, K.; Zhao, H.; Wang, Z.; Zhou, F.; Shi, Z.; Cao, S.; Lan, M. Sandwich-type electrochemical aptasensor based on Au-modified conductive octahedral carbon architecture and snowflake-like PtCuNi for the sensitive detection of cardiac troponin I. *Biosens. Bioelectron.* **2022**, *212*, 114431. [[CrossRef](#)] [[PubMed](#)]
35. Wang, Z.; Zhao, H.; Chen, K.; Li, H.; Lan, M. Sandwich-type electrochemical aptasensor based on hollow mesoporous carbon spheres loaded with porous dendritic Pd@Pt nanoparticles as signal amplifier for ultrasensitive detection of cardiac troponin I. *Anal. Chim. Acta* **2021**, *1188*, 339202. [[CrossRef](#)]
36. Adeel, M.; Rahman, M.; Lee, J.-J. Label-free aptasensor for the detection of cardiac biomarker myoglobin based on gold nanoparticles decorated boron nitride nanosheets. *Biosens. Bioelectron.* **2019**, *126*, 143–150. [[CrossRef](#)]
37. Taghdisi, S.M.; Danesh, N.M.; Ramezani, M.; Emrani, A.S.; Abnous, K. A novel electrochemical aptasensor based on Y-shape structure of dual-aptamer-complementary strand conjugate for ultrasensitive detection of myoglobin. *Biosens. Bioelectron.* **2016**, *80*, 532–537. [[CrossRef](#)] [[PubMed](#)]
38. Shumyantseva, V.V.; Bulko, T.V.; Sigolaeva, L.V.; Kuzikov, A.V.; Archakov, A.I. Electrosynthesis and binding properties of molecularly imprinted poly-o-phenylenediamine for selective recognition and direct electrochemical detection of myoglobin. *Biosens. Bioelectron.* **2016**, *86*, 330–336. [[CrossRef](#)] [[PubMed](#)]
39. Zapp, E.; Westphal, E.; Gallardo, H.; de Souza, B.; Vieira, I.C. Liquid crystal and gold nanoparticles applied to electrochemical immunosensor for cardiac biomarker. *Biosens. Bioelectron.* **2014**, *59*, 127–133. [[CrossRef](#)]
40. Yang, Z.; Wang, H.; Dong, X.; Yan, H.; Lei, C.; Luo, Y. Giant magnetoimpedance based immunoassay for cardiac biomarker myoglobin. *Anal. Methods* **2017**, *9*, 3636–3642. [[CrossRef](#)]
41. Singh, S.; Tuteja, S.K.; Sillu, D.; Deep, A.; Suri, C.R. Gold nanoparticles-reduced graphene oxide based electrochemical immunosensor for the cardiac biomarker myoglobin. *Microchim. Acta* **2016**, *183*, 1729–1738. [[CrossRef](#)]

Disclaimer/Publisher’s Note: The statements, opinions and data contained in all publications are solely those of the individual author(s) and contributor(s) and not of MDPI and/or the editor(s). MDPI and/or the editor(s) disclaim responsibility for any injury to people or property resulting from any ideas, methods, instructions or products referred to in the content.